



1 Quantitative effects of antecedent effective rainfall on *ID* threshold for debris flow

2 Shaojie Zhang ¹, Hongjuan Yang ¹, Dunlong Liu ², Kaiheng Hu¹, Fangqiang Wei¹

3 1. Key Laboratory of Mountain Hazards and Earth Surface Process, Institute of Mountain Hazards and
4 Environment, Chinese Academy of Sciences, Chengdu 610041, China

5 2.College of Software Engineering, Chengdu University of Information and Technology, Chengdu, 610225, China

6 Correspondence to: K.H. Hu, E-mail: khhu@imde.ac.cn, F.Q. Wei, E-mail: fqwei@imde.ac.cn

7

8 Abstract

9 Studies have shown that the antecedent effect precipitation (*AEP*) is closely related to rainfall
10 intensity-duration (*ID*) threshold of debris flow. However, the quantitative relationship between
11 the *AEP* and *ID* threshold is still undetermined. In this study, a hydrological process based
12 numerical model (Dens-*ID*) that can derive the *ID* threshold curve is adopted to address this issue.
13 Jiangjia Gully (JJG) in Dongchuan District of Yunnan Province was chosen as the study area,
14 Dens-*ID* was used to derive a series of *ID* threshold curves corresponding to different *AEP*. Based
15 on calculated data sets including *AEP*, *ID* curves, parameters of *ID* curve equation (α and β), and
16 debris flow density, the influence of *AEP* on the *ID* threshold curve is deeply explored. We found
17 that although solid materials and runoff are the two necessary conditions for the formation of
18 debris flow, the specific roles played in which are different: the volume of loose solid sources
19 provides a basal condition for debris flow and determines the scale of debris flow, while the runoff
20 volume will have a sudden change during the rainfall process, which is a key factor promoting the
21 formation of debris flow. In the condition of *AEP* ranging from 20 mm to 90 mm, *AEP* and α can



be described by the equation $\alpha = -0.0078AEP^2 + 0.68AEP + 6.43$, and β shows a linear change law with AEP . The error of the two equations were evaluated using 45 historical rainfall data that triggered debris flows, which is equal to 37.85% and 11.1%. Due to the two functions, the ID threshold curve can regularly move in the I-D coordinate system rather than a conventional threshold curve stay the same regardless of AEP variation, it is beneficial to improve the prediction capacity of the ID threshold.

1 Introduction

Precipitation that affects debris flow formation includes triggering rainfall and antecedent effective precipitation (AEP) before the event (Chen et al., 2015; Chen et al., 2018; Oorthuis et al., 2021). AEP is precipitation that remains in soil before a debris flow occurs; it reflects the degree of soil saturation (Zhang et al., 2015). Increased AEP, and thus increased moisture content, has been shown to enhance surface rainfall-induced runoff in various environments (Tisdall, 1951; Luk, 1985; Le Bissonnais et al., 1995; Castillo et al., 2003; Jones et al., 2017). Additionally, the increased soil water content caused by AEP decreases the shear strength of the loose soil mass in a debris flow gully, enhancing the supply rate of the solid material required for debris flow formation (Lehmann and Or, 2012; Kim et al., 2013; Ruetten et al., 2014). AEP has an important effect on the rainfall threshold for triggering debris flow. Debris flow prediction can be improved by quantifying this effect (Chen et al., 2018; Zhao et al., 2019; Hirschberg et al., 2021; Marino et al., 2020; Jiang et al., 2021).

A rainfall threshold is generally a fixed value of some rainfall parameter such as cumulative rainfall, hourly rainfall intensity, or AEP (Marra et al., 2017); alternatively, it can be a curve of two rainfall parameters (Peres and Cancelliere, 2014), such as the rainfall intensity–rainfall



44 duration threshold curve (Cain, 1980) and rainfall intensity–antecedent rainfall curve (Long et al.,
 45 2020). The most commonly investigated threshold is the intensity (I) versus duration (D) curve
 46 (Crosta and Frattini, 2003; Cannon et al., 2008; Guzzetti et al., 2008; Berti et al., 2020), which has
 47 the form $I = \alpha D^\beta$, where I represents the average rain intensity in the rainfall process that triggers
 48 debris flow, D represents the rainfall duration, and α and β are empirical parameters. Segoni et al.
 49 (2018) analyzed the rainfall thresholds of landslides and debris flows reported in 107 articles and
 50 found that the threshold model based on the ID threshold curve accounted for the highest
 51 proportion, approximately 48.6%. Empirical and process-based methods are commonly used to
 52 derive the ID threshold curves of debris flow (Segoni et al., 2018). The empirical model workflow
 53 is as follows. Data on debris flow events and the associated rainfall in a target area are collected,
 54 and the I and D values of each rainfall process that triggered a debris flow event are calculated. D
 55 and I are plotted on the x and y axes, respectively, and the ID threshold curve is fitted using these
 56 data. As for the process-based methods, a typical physical parameter (P_i) that can represent debris
 57 flow occurrence in a gully is first chosen, and the change in this parameter has a certain threshold
 58 interval (e.g., $[P_{\text{low}}, P_{\text{upper}}]$). During a rainfall process, P_i changes because of hydrological
 59 processes such as rainfall infiltration and runoff. When it falls into the interval $[P_{\text{low}}, P_{\text{upper}}]$, a
 60 debris flow may be triggered under these rainfall conditions. Then a numerical model is built to
 61 calculate P_i by inputting different rainfall conditions characterized by different D and I . For a
 62 certain value of P_i (e.g., P_{upper}), the $[D_i, I_i]$ data for which the calculated value is equal to P_{upper} are
 63 collected during model calculations. These collected data are then used to fit the threshold curves
 64 (Long et al., 2020). Papa et al. (2013) proposed that the total area (S) of shallow landslides
 65 induced by rainfall in a gully plays an important role in debris flow formation. Therefore, the ratio



66 of S to the catchment area is used as the threshold (that is, P_i), and the **TRIGERS** model (Baum et
 67 al., 2002, 2008) and a rainfall scenario simulation are adopted to calculate P_i and search for the
 68 combination of all $[I_i, D_i]$ at which the P_i calculated by the model is equal to a preset value. Next,
 69 the ID threshold curve corresponding to this value is obtained by fitting. Although shallow
 70 landslides induced by rainfall in a basin are very important for debris flow formation, the effect of
 71 hydrodynamic conditions provided by rainfall-induced runoff on debris flow formation cannot be
 72 ignored. Scholars have argued that a water-soil mixture in a gully can be formed by coupling
 73 between the rainfall-induced solid material and runoff (Church and Jakob, 2020). The debris flow
 74 density represents the fluid characteristics of the mixture and can be used to incorporate the two
 75 major factors (rainfall-induced loose solid material and rainfall-induced runoff) that affect debris
 76 flow formation into numerical simulation models (Zhang et al., 2020; Long et al., 2020). A
 77 numerical model (Dens-ID) is used to correlate rainfall parameters with the density boundaries of
 78 **1.2 and 2.2 g/cm³**; the ID threshold curve of debris flow can then be constructed in the physical
 79 framework. The ID curve fitted by this model reportedly has a shape similar to that of the
 80 statistics-based curve. The precision of debris flow prediction by this model in Jiangjia Gully (JJG)
 81 in Yunnan Province, China, is approximately 80.5%, which is 27.7% higher than that of the
 82 statistics-based ID curve (Zhang et al., 2020).

83 It is difficult to introduce AEP as a dependent variable into the power function $I = \alpha D^\beta$.
 84 Attempts to analyze the effect of AEP on the parameters α and β have resulted in the following
 85 **consensus**. A larger AEP **can decrease the rainfall conditions triggering debris flow**; however, an
 86 equation that describes the quantitative evolution of each parameter (α or β) with AEP has not
 87 been derived. Some studies have used the relationship between daily rainfall and antecedent



88 rainfall (Kim et al., 1991; Glade et al., 2000; Dahal and Hasegawa, 2008; Giannecchini et al.,
89 2012) or a combination of daily rainfall intensity and rainfall duration (Hasnawir and Kubota,
90 2008; Khan et al., 2012; Zhao et al., 2019; Kim et al., 2020; Yang et al., 2020) to investigate the
91 effects of AEP on the rainfall threshold. Jiang et al. (2021) investigated the probabilistic rainfall
92 thresholds for debris flows after the Wenchuan earthquake and found that antecedent precipitation
93 plays an important role in long-duration rainfall-induced debris flows. Zhao et al. (2019)
94 introduced the simulated antecedent soil moisture into a probabilistic threshold and found that it
95 exhibited better prediction performance than the daily rainfall intensity and rainfall duration (*ED*)
96 threshold. However, all of these studies lack a quantitative description of the effect of AEP on the
97 rainfall threshold. This lack is attributed mainly to the absence of sufficient historical data
98 including AEP, rainfall intensity, rainfall duration, and debris flow events, which makes it difficult
99 to conduct differential analysis and to derive a function that quantitatively describes their
100 relationship.

101 To quantify the effect of AEP on the *ID* threshold curve, JJG in Yunnan Province, China, was
102 chosen as the study area, and the Dens-ID numerical model was used to build its *ID* threshold
103 curve database. The mechanism by which AEP affects the *ID* threshold curve is thoroughly
104 discussed using this database, and equations for the functions describing the relationships between
105 AEP and the parameters α and β were derived through data analysis.

106 2 Methods

107 2.1 Dens-ID

108 Shallow landslides and bed erosion are the two main sources of debris flow material; both



may be present in the same gully, but one type is always dominant (Gabet and Mudd, 2006; Berti and Simoni, 2005; Coe et al., 2008; Long et al., 2020). Debris flow gullies with shallow landslides as the source of solid materials are widely distributed in southwestern China (Zhang et al., 2020). **Dens-ID** focuses on landslide-dominated supply and is designed to derive the *ID* threshold curves of debris flow by calculating the debris flow density in rainfall scenario simulations. The key function of this model is to correlate debris flow density with rainfall parameters, as described by Zhang et al. (2020) and Long et al. (2020). Debris flows are complex mixtures of water, fragmented rock, and sediments of all sizes (Chmiel et al., 2020). Dens-ID simplifies this complex nonuniform flow (Iverson, 1997) as a water-soil mixture. The runoff amount $[V_w(t)]$ and amount of solid material $[V_s(t)]$ are taken as the two parameters contributing to debris flow formation. Using these two parameters as the inputs of Eq. 1, Dens-ID can calculate the density of the water-soil mixture.

$$\rho_{mix}(t) = \frac{\rho_w V_w(t) + \rho_s V_s(t)}{V_{mix}(t)} \quad (1)$$

where $\rho_{mix}(t)$ is the density of the water-soil mixture, ρ_w is the water density, ρ_s is the density of soil particles, and $V_{mix}(t)$ is the volume of the water-soil mixture, which is the sum of $V_w(t)$ and $V_s(t)$. $V_w(t)$ and $V_s(t)$ are the key variables for correlating the debris flow density with the rainfall parameters, which can be derived by pixel-based hydrological simulation (Long et al., 2020).

Based on a digital elevation model (DEM) of a debris flow gully, Dens-ID uses the theory of runoff generation from excess precipitation to control the infiltration boundary in the topsoil (Zhang et al., 2014a). It then simulates the vertical water movement within the soil mass using the differential equation of Richards (1931).



130 Governing equation of infiltration border: $-D(\theta) \frac{\partial \theta}{\partial z} + K(\theta) = I(t)$ (2)

131 Richards' differential equation: $\frac{\partial \theta}{\partial t} = \frac{\partial}{\partial z} [D(\theta) \frac{\partial \theta}{\partial z}] - \frac{\partial K(\theta)}{\partial \theta}$ (3)

132 where θ is the soil water content; $D(\theta) = K(\theta)/(d\theta/d\psi)$ is the soil water diffusivity; z is the soil
 133 depth, which is positive downward along the soil depth, taking the topsoil as the origin; $K(\theta)$ is
 134 the hydraulic conductivity; $I(t)$ is the rainfall intensity; and ψ is the soil matric suction.

135 After the hydrological simulation, Dens-ID outputs the water soil content $\theta(i, t)$, soil matric
 136 suction $\psi(i, t)$, and runoff depth $dw(i, t)$ for each pixel of the DEM. Dens-ID then calculates $V_w(t)$
 137 using the runoff depth $dw(i, t)$, as shown in Eq. 4.

138
$$V_w(t) = \sum_{i=1}^T \sum_{j=1}^n S_g * dw(i, t)$$
 (4)

139 where n represents the total number of grid cells that can generate runoff at time t , and $V_w(t)$
 140 represents the total volume of runoff in a gully at time t . Using $\theta(i, t)$ and $\psi(i, t)$ as inputs, Dens-ID
 141 adopts an infinite slope model (Zhang et al., 2014b; Liu et al., 2016; Zhang et al., 2018) to
 142 calculate the unstable depth of each grid cell $ds(j, t)$. It then calculates $V_s(t)$ using $ds(j, t)$, as shown
 143 in Eq. 5.

144
$$V_s(t) = \sum_{i=1}^T \sum_{j=1}^m S_g * ds(j, t)$$
 (5)

145 where m represents the number of grid cells that can provide solid material at time t , and $V_s(t)$ is
 146 the total volume of solid material in the gully at time t .

147 The mixture density can be derived by substituting various rainfall parameters, including
 148 rainfall intensity (I) and rainfall duration (D), into the right side of Eq. 2. Then Dens-ID can
 149 correlate the rainfall parameters with the debris flow density.

150 2.2 Derivation of ID threshold curve using Dens-ID



151 The debris flow density varies between 1.2 and 2.3 g/cm³. The values within the interval [1.2,
 152 2.3] represent a density set. In nature, a debris flow with a density ρ_{mix} cann be triggered by high-
 153 intensity or long-duration rainfall. Inputting rainfall scenarios with different combinations of [I_i ,
 154 D_i] into Dens-ID makes it possible to simulate debris flow initiation by rainfall in nature. Using a
 155 given density value (ρ_{mix}) during the calculation, Dens-ID collects all the [I_i , D_i] data that meet the
 156 conditions of the rainfall scenarios (Fig. 1). That is, when the selected [I_i , D_i] are used as input,
 157 the output of the model is equal to ρ_{mix} . The collected [I_i , D_i] values represent another data group,
 158 which is referred to as a rainfall parameter set. Each data point [I_i , D_i] corresponds to a unique
 159 value of ρ_{mix} within the density set; thus, the correlation between the rainfall parameters and debris
 160 flow density can then be established by Dens-ID. An ID curve can then be fitted through the
 161 collected [I_i , D_i] data to show the relationship between I and D . Each fitted ID curve corresponds
 162 to a unique ρ_{mix} within the density set, which is also considered to be the isodensity line (Zhang et
 163 al., 2020). Two values close to the left and right boundaries are chosen from the density set as ρ_{mix} ,
 164 and the ID threshold curve corresponding to these two density values can represent the lower and
 165 upper boundaries for debris flow formation. The ID curves corresponding to a density value ρ_{mix}
 166 are fitted as follows:

167 Step 1: Assign values of 1.2 and 2.2 g/cm³ to ρ_{mix} .

168 Step 2: Assign a value to the AEP. In nature, the AEP represents the antecedent soil moisture
 169 before the rainfall process that may trigger a debris flow. In Dens-ID, the natural debris flow gully
 170 is divided into a series of grid cells, and the AEP represents the soil moisture content of each grid
 171 cell before rainfall infiltration. Using the initial hydrological conditions represented by the AEP,
 172 Dens-ID simulates hydrological processes such as runoff and infiltration during the triggering



precipitation process. To quantitatively analyze the effect of AEP on the ID threshold curve, AEP_i was assigned values of 10, 20, 30, 40, 50, 60, 70, 80, 90, 100, 110, and 120 mm.

Step 3: Assign a value to I_i , which generally represents the average rainfall intensity of a rainfall process that can trigger a debris flow and is held constant until the calculations in Step 4 are complete. The initial value of I_i is set to 1 mm/h. When Step 4 is complete, I_i is increased by 0.5 up to I_{\max} . At I_{\max} , a debris flow with density ρ_{mix} can be triggered in the gully when $D = 1$.

Step 4: Under constant I_i , the calculation time of the model starts at $t = 1$ h and increases by 1 h at each calculation step until $t = D_i$, where D_i represents the rainfall duration required to trigger a debris flow with density ρ_{mix} . After $t = D_i$, the model calculation for a given I_i is complete.

Step 5: Repeat Steps 3 and 4 and collect the I_i and D_i values at which Dens-ID outputs the pre-set ρ_{mix} . When the rainfall intensity I_i increases to I_{\max} , the calculation for a given AEP_i is complete. Thus, the data set of I_i and D_i for a certain AEP_i is obtained, and the corresponding ID threshold curve can be fitted using these data.

Step 6: Repeat Steps 2, 3, 4, and 5, and collect the I_i and D_i values. When AEP reaches 120 mm, the calculation for a given ρ_{mix} is complete.

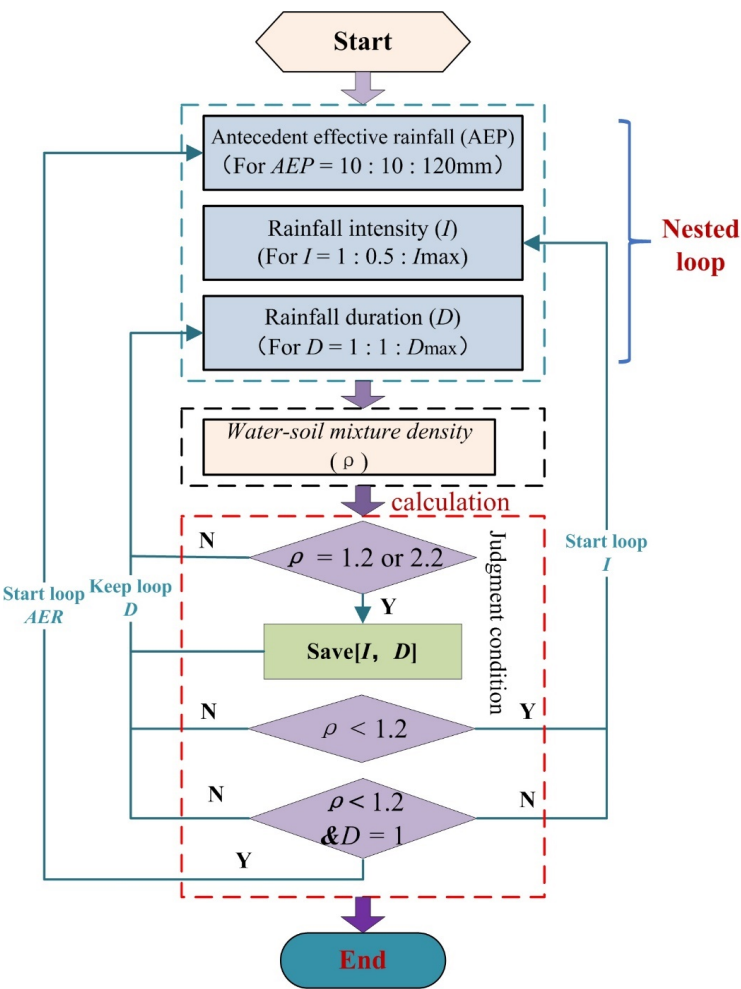


Fig. 1 Flow chart of model calculation for obtaining $[I, D]$ data

3 Study area and data collection

3.1 Jiangjia Gully

JJG is located in the Dongchuan district of Kunming City, Yunnan Province, China, and is the primary tributary of the Xiaojiang River. JJG has a drainage area of 48.6 km², and its elevation ranges from 1040 to 3260 m (Fig. 2). The terrain in JJG is steep; the relative relief between the ridge and valley is approximately 500 m, and most slopes have a gradient exceeding 25°. Menqian



196 and Duozhao gullies, which are shown in Fig. 2, are the two main tributaries and account for
 197 64.7% of the entire drainage area. These two tributaries constitute the initiation zones of debris
 198 flow in JJG, and their channels are typically narrow and V-shaped [Fig. 3(c)]. JJG is characterized
 199 by intense tectonism, and approximately 80% of the exposed rocks are highly fractured and
 200 slightly metamorphosed. The predominant sandstone and slate can be easily identified by their
 201 light and dark colors, respectively. Both rock types are weak and easily weathered and fragmented
 202 (Yang et al., 2020).

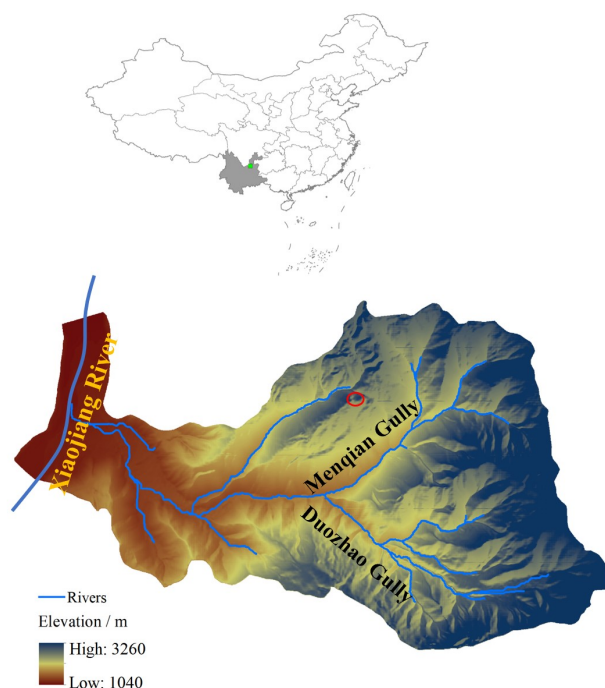


Fig. 2 Location of JJG

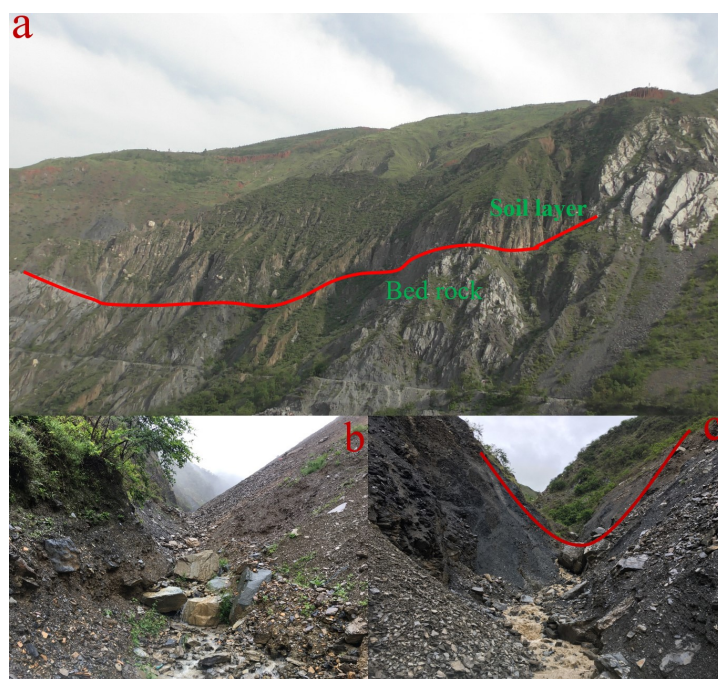


Fig. 3 Loose solid material in JJG

The slopes on both sides of JJG are covered by a loose soil mass tens of meters in thickness [Fig. 3(a)]. Because of intense rainfall, shallow landslides frequently occur on the slopes and provide a large amount of loose solid material for debris flows [Fig. 3(b)]. The steep terrain and large amount of loose solid material in JJG provide suitable conditions for debris flow formation. According to the collected rainfall data, high-intensity or long-duration rainfall can trigger debris flow events (Guo et al., 2013; Zhang et al., 2020). The solid material in JJG originates mainly from shallow landslides, which is consistent with the model assumptions. Therefore, JJG is chosen as the study area to quantitatively examine the effect of AEP on the *ID* threshold curves of debris flows.

3.2 Data for model calculation and validation

◆ Terrain data



DEM data for JJG were provided by the Dongchuan Debris Flow Observation and Research Station. The spatial resolution of the DEM is 0.5 m, and the data were obtained in December 2017 by aerial photogrammetry using an unmanned aerial vehicle. A DEM with a grid size of 10 m was generated from the original terrain data using the resampling tools in ArcGIS, which were used to derive the geometrical parameters of JJG such as slope length, gradient, and river channels.

◆ Data necessary for hydrological simulation

Three main soil types (Table 1) occur in the JJG: dry red soil, red-yellow soil, and gravelly soil. Gravelly soil is widely distributed upstream in JJG and is the main source of solid material for debris flow. The hydrological parameters listed in Table 1 were obtained from the National Soil Database. The grid size of the land use map is 250 m, and its parameters, such as the normalized difference vegetation index, were obtained from the Moderate Resolution Imaging Spectroradiometer database. These data related to hydrological parameters were converted into a map with an accuracy comparable to that of the DEM using the resampling tool in ArcGIS.

Table 1 Soil types and their hydrological parameters

Soil type	θ_s	θ_r	Parameters of curve		f_s (mm/h)
			α	n	
Gravelly soil	0.54017	0.07639	0.02201	1.37785	30.486
Red-yellow soil	0.48519	0.06829	0.02264	1.38146	21.964
Dry red soil	0.48148	0.07640	0.01476	1.47394	10.811

◆ Soil mechanical parameters

Eq. 7 (section 4.3) can be used to determine two soil mechanical parameters, soil cohesion c and internal friction angle φ , by direct shear tests of soil samples from JJG. Most of the solid material for debris flows in JJG originates from gravelly soil; therefore, three groups of soil samples were taken from several typical slopes covered by a gravelly soil mass, and one sample each was taken from the red-yellow and dry red soil. As shown in Table 2, the three samples from



238 gravelly soils have similar c and ϕ values; therefore, the average values of the two parameters
 239 were calculated to represent the mechanical performance of the gravelly soil mass. The
 240 mechanical parameters in Table 2 can be assigned to each grid cell of the DEM according to the
 241 distribution of soil types in JJG.

242 Table 2 Cohesion c and internal friction angle ϕ of soil samples from JJG

Soil samples	Soil mechanical parameter			
	c (kPa)	ϕ (deg)	Average c (kPa)	Average ϕ (deg)
Gravelly soil-1	35.1	36.0	34.5	34.4
Gravelly soil-2	35.9	33.7		
Gravelly soil-3	32.5	33.7		
Red-yellow soil	27.0	36.3	27.0	36.3
Dry red soil	25.9	35.7	25.9	35.7

243 ♦ Historical debris flow and rainfall data

244 To validate the quantitative relationship between the AEP and the ID threshold curves of
 245 debris flows, data for 45 debris flow events in JJG and the triggering rainfall processes were
 246 collected. Rainfall events must be separated from long-term rainfall sequences to identify the
 247 rainfall processes that triggered the 45 debris flow events. The inter-event time (IET) was defined
 248 as a measure of the minimum time interval between two consecutive rainfall pulses (Adams et al.,
 249 1986). Although the IET strongly affects the start and end times of an event (Bel et al., 2017),
 250 there are no standard criteria for rainfall episode separation (Jiang et al., 2021). Peres et al. (2018)
 251 noted that the IET depends on whether the rainfall during an IET is smaller than the mean daily
 252 potential evapotranspiration (MDPE). Long-term observation of the evaporation in JJG showed
 253 that the MDPE in this gully is approximately 4 mm; thus, precipitation of less than 0.5 mm during
 254 an IET is considered to indicate the end of a rainfall process.



The AEP was calculated as the weighted sum of rainfall periods before a debris flow (Long et al., 2020) and is expressed as follows:

$$AEP = \sum_{i=1}^n K^n R_i \quad (6)$$

where the AEP is the antecedent effective rainfall; K is the attenuation coefficient, which is equal to 0.78 according to a field test in JJG (Cui et al., 2003); and n is the number of days preceding the debris flow. Table 3 lists the calculated AEP, average rainfall intensity (I), and rainfall duration (D) of each debris event. The calculated AEP values in the third column of Table 3 are rounded to integers to increase the number of debris flow events corresponding to each AEP. AEP values of 90 and 60 mm are associated with 1 debris flow event each, 8 events have an AEP value of 40 mm, 13 events have an AEP value of 30 mm, 14 events have an AEP value of 20 mm, and 8 events have an AEP value of 15 mm.

Table 3 Historical data of debris flow events and rainfall

Number	Date	AEP	Rounded AEP	Rainfall duration (h)	Intensity (mm/h)
1	2004/7/9	92.60	90	9.30	1.00
2	2001/6/29	59.30	60	4.50	6.70
3	2008/7/5	44.77	40	8.88	1.97
4	2001/7/4	42.50		21.7	1.40
5	2001/7/8	39.80		6.8	3.80
6	2008/8/7	39.73		27.10	1.58
7	2008/6/15	38.87		16.90	1.43
8	2007/7/24	38.35		6.05	2.89
9	1999/8/25	36.20		7.8	3.10
10	2006/7/6	35.20		2.27	10.37
11	1999/7/16	34.00	30	4	11.8



12	2008/7/21	33.47		10.43	2.65
13	2000/8/9	31.60		2.3	8.6
14	2008/8/3	31.35		7.25	3.14
15	2010/7/17	30.385		1.00	4.6
16	2001/6/27	30.30		4	13.1
17	2007/9/17	30.15		9.38	2.44
18	2001/8/13	29.80		3.2	5.3
19	1994/6/26	29.00		2	23
20	2008/7/31	28.99		6.93	2.18
21	1999/7/24	28.90		4.8	9.80
22	2001/8/22	28.00		3.50	6.00
23	2008/8/17	26.29		3.75	3.23
24	2006/8/20	24.63	20	3.15	2.32
25	1999/8/10	23.60		14.20	4.30
26	2000/8/8	23.50		5.20	8.50
27	2008/7/1	23.22		9.88	2.60
28	2000/8/29	22.70		6.00	6.20
29	2010/7/6	22.376		10.88	4.18
30	2008/7/11	21.33		1.85	6.43
31	2006/8/15	20.62		3.08	9.79
32	2006/7/5	20.52		2.32	10.53
33	2000/7/15	19.60		26.2	2.90
34	1993/8/29	18.60		6.70	4.60
35	1998/8/2	18.40		3.70	7.30
36	2004/6/26	18.10		3.50	5.00
37	2007/8/24	16.69		28.60	1.77
38	2007/8/11	14.63	15	6.80	1.88
39	2007/7/10	14.40		1.48	7.01



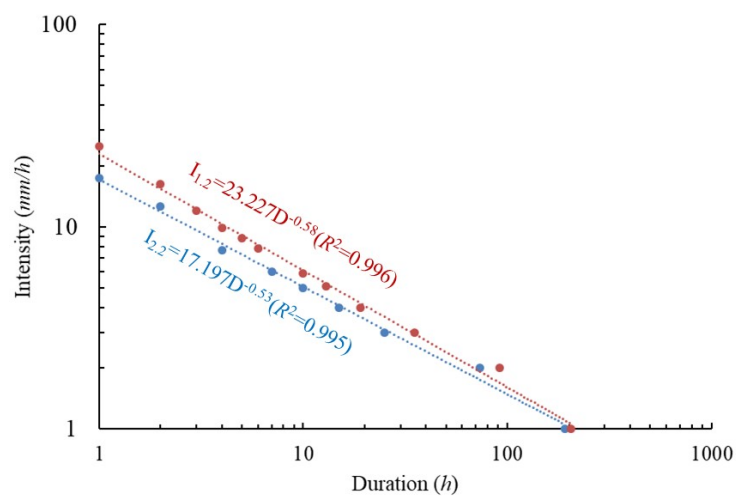
40	2001/6/26	13.40		3.90	11.80
41	2004/7/19	12.60		2.00	9.80
42	1994/6/15	12.50		8.70	6.10
43	1993/8/26	12.10		8.7	3.60
44	2009/8/4	11.90		5.72	9.34
45	2010/9/10	11.51		6.03	5.55

267

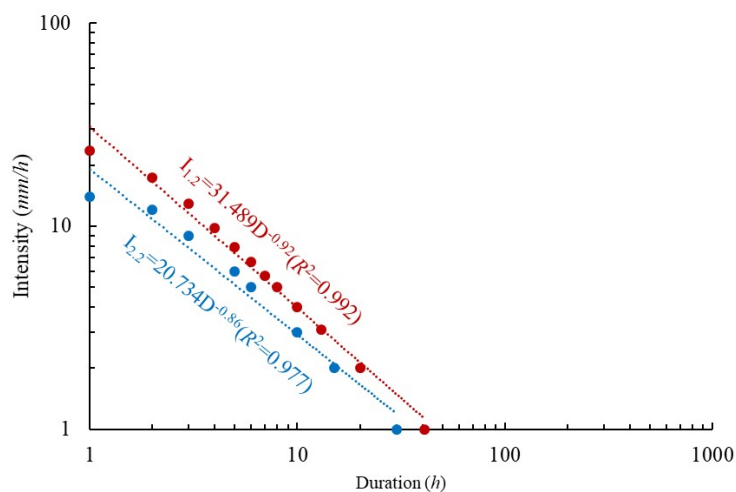
268 4 Results and Discussion

269 4.1 ID threshold curves of debris flow with different AEP

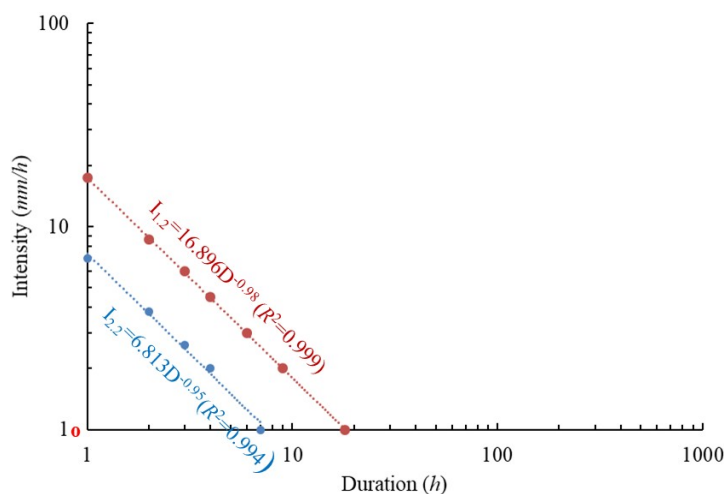
270 Fig. 4 shows three sets of *ID* threshold curves for debris flows with AEP values of 20, 60,
 271 and 10 mm. All of the axes are given on a logarithmic scale. As shown in Fig. 4(a) (AEP = 20
 272 mm), two *ID* threshold curves corresponding to $\rho_{mix} = 1.2$ and $\rho_{mix} = 2.2$ g/cm³ constitute the
 273 boundaries of the rainfall threshold that triggers debris flow in JJG. The *ID* threshold curves in Fig.
 274 4 can be described by a power function; this result is consistent with the shape of the threshold
 275 curve obtained by the statistical model, indicating that our model can describe the hydrological
 276 process of rainfall-induced debris flow. The *ID* threshold curve corresponding to a density of 2.2
 277 g/cm³ is located below the curve that corresponds to a density of 1.2 g/cm³, indicating that debris
 278 flows with higher density are more easily triggered in JJG. AEP has a significant qualitative effect
 279 on the *ID* threshold curve of a debris flow. Essentially, a large AEP value indicates that the rainfall
 280 requirements for rainfall-induced debris flow are low. For $D = 1$ h, the rainfall intensity I that can
 281 trigger a debris flow with a density of 1.2 g/cm³ decreases from 26.2 to 16.7 mm/h with increasing
 282 AEP. The trend revealed by this calculation result is essentially consistent with the results of field
 283 observations in JJG (Cui et al., 2003).



(a) AEP = 20 mm



(b) AEP = 60 mm



(c) AEP = 100 mm

Fig. 4 ID threshold curves of debris flow for different AEP values

In addition, Fig. 4 shows that the distance between the two ID threshold curves becomes larger with increasing AEP, indicating a higher occurrence probability of rainfall-induced debris flow. A database including all the data sets, including $[I, D]$, the fitted curves, and AEP (Table 4) was used to quantitatively analyze the effect of AEP on the threshold curve.

Table 4 Database of AEP, fitted equations, and $[I, D]$ data groups

AEP (mm)	Fitted threshold curves of debris flow in JJG	
	1.2 g/cm ³	2.2 g/cm ³
10	$I_{1.2} = 19.851D^{-0.54} D \in [1, 269] (R^2 = 0.991)$	-
15	$I_{1.2} = 21.69D^{-0.55} D \in [1, 236] (R^2 = 0.993)$	$I_{2.2} = 16.10D^{-0.50} D \in [1, 229] (R^2 = 0.995)$
20	$I_{1.2} = 23.227D^{-0.58} D \in [1, 203] (R^2 = 0.996)$	$I_{2.2} = 17.197D^{-0.531} D \in [1, 192] (R^2 = 0.995)$
30	$I_{1.2} = 26.24D^{-0.64} D \in [1, 143] (R^2 = 0.996)$	$I_{2.2} = 18.087D^{-0.57} D \in [1, 132] (R^2 = 0.995)$
40	$I_{1.2} = 40.589D^{-0.78} D \in [1, 103] (R^2 = 0.966)$	$I_{2.2} = 22.154D^{-0.64} D \in [1, 92] (R^2 = 0.984)$
50	$I_{1.2} = 41.263D^{-0.86} D \in [1, 65] (R^2 = 0.981)$	$I_{2.2} = 23.501D^{-0.74} D \in [1, 55] (R^2 = 0.980)$
60	$I_{1.2} = 31.489D^{-0.92} D \in [1, 40] (R^2 = 0.992)$	$I_{2.2} = 20.734D^{-0.86} D \in [1, 30] (R^2 = 0.977)$

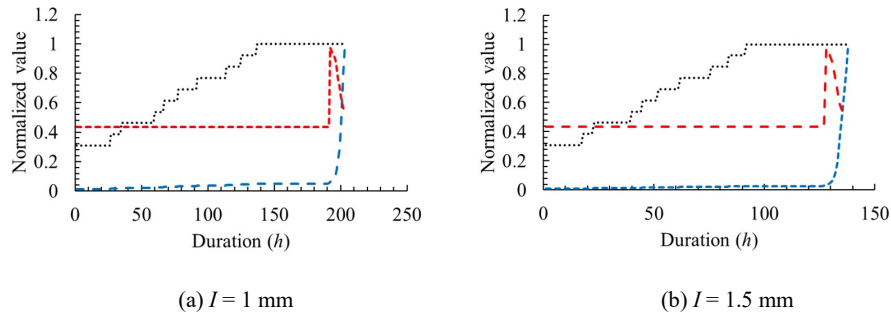


70	$I_{1.2} = 23.049D^{-0.96} D \in [1, 25] (R^2 = 0.9983)$	$I_{2.2} = 13.042D^{-0.93} D \in [1, 15] (R^2 = 0.995)$
80	$I_{1.2} = 18.719D^{-0.98} D \in [1, 20] (R^2 = 0.997)$	$I_{2.2} = 9.960D^{-0.95} D \in [1, 11] (R^2 = 0.999)$
90	$I_{1.2} = 16.991D^{-0.98} D \in [1, 18] (R^2 = 0.999)$	$I_{2.2} = 6.813D^{-0.95} D \in [1, 7] (R^2 = 0.994)$
100	$I_{1.2} = 16.896D^{-0.98} D \in [1, 18] (R^2 = 0.999)$	$I_{2.2} = 6.813D^{-0.95} D \in [1, 7] (R^2 = 0.994)$
110	$I_{1.2} = 16.873D^{-0.98} D \in [1, 16] (R^2 = 0.999)$	$I_{2.2} = 6.755D^{-0.95} D \in [1, 7] (R^2 = 0.997)$
120	$I_{1.2} = 16.873D^{-0.98} D \in [1, 16] (R^2 = 0.999)$	$I_{2.2} = 6.755D^{-0.95} D \in [1, 7] (R^2 = 0.997)$

Note that Dens-ID cannot collect sufficient $[I_i, D_i]$ data for fitting the ID threshold curve for a density of 2.2 g/cm³ and AEP = 10 mm. At this low AEP value, the supply rate of solid material is lower than the runoff rate; thus, it is difficult to trigger a high-density debris flow in JJG. By contrast, for AEP ≥ 90 mm, α and β tend to be constant. The AEP can significantly affect the ID curves of debris flow in JJG at values of 10 to 90 mm.

4.2 Effects of loose solid material and runoff on debris flow formation

In Dens-ID, the parameters $V_w(t)$ and $V_s(t)$ in Eq. 1 are the process variables for calculating the density of the water-soil mixture. Because the ID threshold curves in Fig. 4 are all related to the debris flow density, it is necessary to analyze the relationship between debris flow density and $V_w(t)$ and $V_s(t)$ under different rainfall conditions.



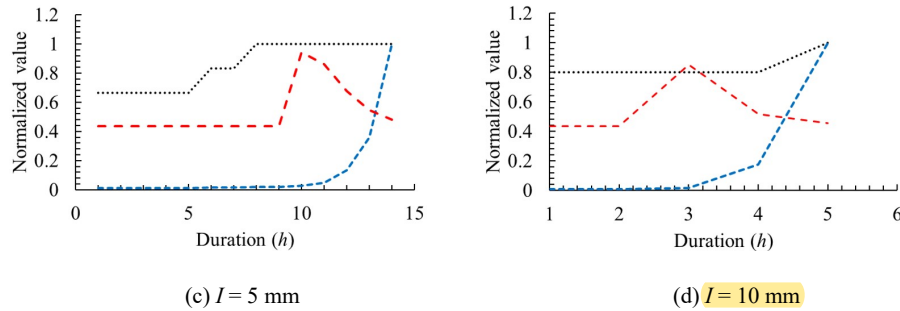


Fig. 5 Process graphs of $V_s(t)$, $V_w(t)$, and $\rho_{mix}(t)$ for different rainfall intensity values I and AEP = 20 mm.

Black dotted line represents the volume variation of $V_s(t)$, blue dotted line represents the volume variation of $V_w(t)$, and red dotted line represents the density of the water-soil mixture.

Fig. 5 shows process graphs of $V_s(t)$, $V_w(t)$, and $\rho_{mix}(t)$ for different rainfall intensity values I at AEP = 20 mm. Because these three parameters have different magnitudes, they were normalized to better show their dynamic evolution.

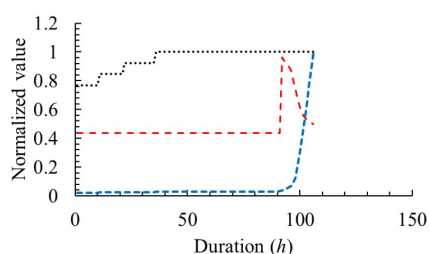
The red curve represents the debris flow density for different rainfall intensity values I , which reveals a clear water process (Stage 1), debris flow phase (Stage 2), and hyperconcentrated flow stage (Stage 3). In Stage 1, the runoff rate is lower than the supply rate of solid material (black dotted line) in JJG. During this stage, the runoff in JJG cannot provide hydrodynamic conditions suitable for transporting these loose deposits, and no debris flow occurs. In Stage 2, during continuous hydrological processes such as rainfall infiltration and runoff generation, the total volume of runoff ($V_w(t)$) in JJG increases rapidly, and the blue dotted lines in Fig. 5(a)–(d), which represent the volume variation of $V_w(t)$, all show a sharp increase. Consequently, the hydrodynamic conditions are sufficient for debris flow formation. The rainfall-induced loose solid material and runoff in the channel can be fully coupled, and thus a debris flow can be triggered. In Stage 3, a sudden increase in runoff volume and decrease in the supply rate of loose solid material



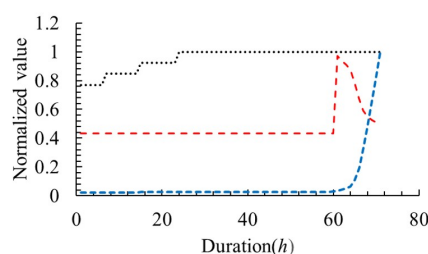
327 cause the debris flow in JJG to quickly become hyperconcentrated. Therefore, the red dotted line
 328 in Fig. 5 also shows that debris flows generally begin suddenly but quickly reach Stage 3 because
 329 of the rapid increase in runoff.

330 The black dashed line in Fig. 5 represents the variation of $V_s(t)$. The hydrological conditions
 331 represented by AEP = 20 mm induce shallow landslides in JJG before rainfall begins. In the initial
 332 stage of the rainfall process, the supply rate of solid material is higher than the runoff rate in JJG;
 333 however, as the rainfall process continues, the supply rate is overtaken by the runoff rate, and the
 334 total volume stabilizes at a maximum value.

335 The blue dashed lines in Fig. 5 represent the variation of $V_w(t)$. They all show a sharp
 336 increase at a certain time, at which debris flows also occur. Thus, the sudden occurrence of debris
 337 flows is caused mainly by increasing runoff. These results indicate that the supply of loose solid
 338 material is essential to debris flow formation, but the decisive factor in debris flow occurrence is
 339 the sharp increase in runoff.



(a) $I = 1 \text{ mm}$



(b) $I = 1.5 \text{ mm}$

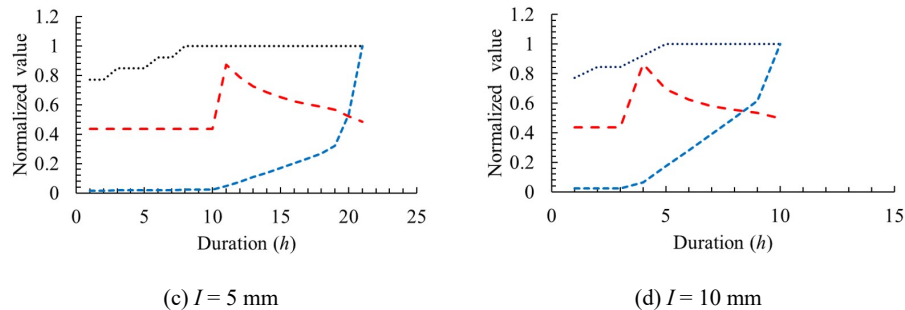


Fig. 6 Process graphs of $V_s(t)$, $V_w(t)$, and $\rho_{mix}(t)$ for different rainfall intensity values I and AEP = 40 mm.

Black dotted line represents the volume variation of $V_s(t)$, blue dotted line represents the volume variation of $V_w(t)$, and red dotted line represents the density of the water-soil mixture.

4.3 Quantitative analysis of effects of AEP on α and β

The three ID curves from Fig. 4 corresponding to a density of 2.2 g/cm^3 and different AEP values are plotted in Fig. 7 to further examine the variation of the ID curves with AEP. The AEP can change the position of the ID threshold curve in the I - D coordinate system, indicating that a higher AEP value shifts the ID threshold curve closer to the origin. This tendency is consistent with the general consensus that higher AEP can decrease the triggering rainfall conditions (De Vita et al., 2000; Cui et al., 2003; Bel et al., 2017). Consequently, considering the landslide-dominated solid resource supply in JJG, Dens-ID describes the formation process of rainfall-induced debris flow reasonably well. In addition, compared to the range of rainfall intensity I (Y axis), the rainfall duration D (X axis) changes more dramatically with AEP and can quickly decrease from 192 h (AEP = 20 mm) to 7 h (AEP = 100 mm).

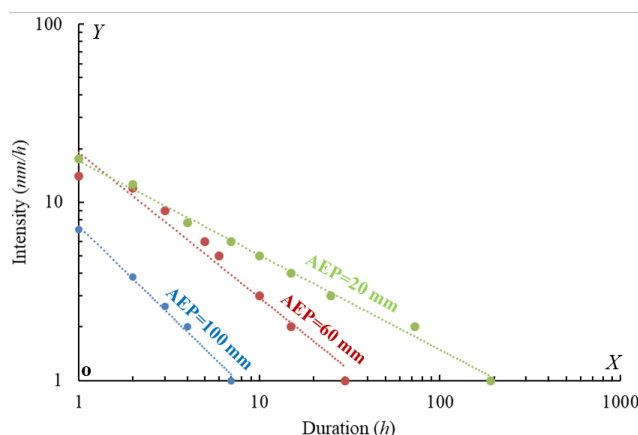


Fig. 7 ID curves corresponding to a density of 2.2 g/cm^3 and AEP values of 20, 60, and 100 mm

The parameters of the ID threshold curve of debris flow, α and β , determine the position of the fitting curve in I - D coordinates. Therefore, it can be deduced that α and β depend on AEP. In this section, the data sets from Dens-ID are used to derive the functional relationships between AEP and these two parameters. First, it is necessary to clarify the physical meaning of α and β . Under the numerical simulation conditions of this study, the variation interval of the independent variable D in the formula $I = \alpha D^\beta$ is $[1, D_{\max}]$, and the variation interval of I is $[I_{\max}, 1]$. According to the formula, when D is equal to 1 h, $I = \alpha$. When $D = 1$, the rainfall duration required to trigger a debris flow is 1 h, and the rainfall intensity I reaches the maximum value, I_{\max} . Therefore, the combination of D and I under these conditions represents high-intensity rainfall. According to this analysis, α is numerically equal to the value of I_{\max} , and thus this parameter represents the critical rainfall intensity required to trigger a debris flow for $D = 1 \text{ h}$.

Before the physical meaning of β is discussed, the expression $I = \alpha D^\beta$ needs to be written logarithmically, as follows:

$$\log I = \log \alpha + \beta \log D \quad (7)$$

By denoting $\log I$ as Y_I , $\log D$ as X_D , and $\log \alpha$ as B_α , Eq. 7 can be rewritten as follows:



$$Y_I = \beta X_D + B_a \quad (8)$$

X_D and Y_I are related to I and D and are independent variables with ranges of $[\log 1, \log(D_{\max})]$ and $[\log 1, \log(I_{\max})]$, respectively. The rewritten equation is represented by a linear equation in Figs. 4 and 5, where β is the slope of each line and is less than 0. The main reason that β is less than 0 is a tradeoff between rainfall intensity and rainfall duration in nature, which facilitates the occurrence of debris flow. The absolute value of β represents the deceleration rate of rainfall intensity with increasing rainfall duration, that is, the rate of decrease from I_{\max} to 1 mm/h. The α and β values in Table 4 can be classified into two groups according to debris flow density (1.2 or 2.2 g/cm³). The α and β values in the two groups show similar variation with AEP. Thus, one data group (Table 5) corresponding to a density of 2.2 g/cm³ was selected to examine the effect of AEP on α and β .

Table 5 Calculated α and β for different AEP values

Fitting para- meter	AEP (mm)											
	10	20	30	40	50	60	70	80	90	100	110	120
α	-	17.2	18.1	22.2	23.5	20.7	13.0	9.9	6.8	6.8	6.8	6.8
β	-	-0.53	-0.57	-0.64	-0.74	-0.86	-0.93	-0.95	-0.95	-0.95	-0.95	-0.95

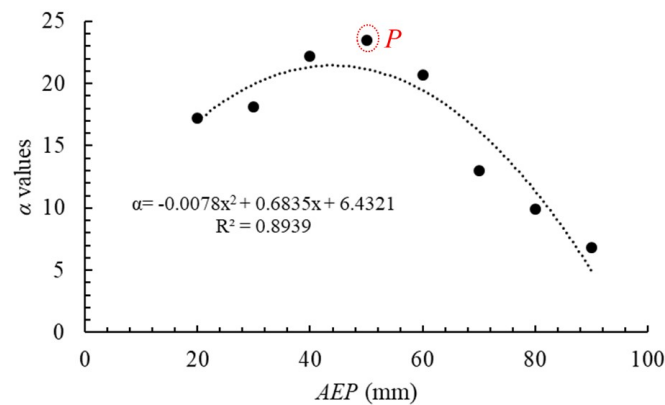
Effect of AEP on α : The effect of AEP on α is described by the following equations, which were fitted using the AEP and α values in Table 5:

$$\begin{cases} \alpha = -0.0078AEP^2 + 0.68AEP + 6.43 & 20 \leq AEP < 90 \\ \alpha = 6.8 & 90 \leq AEP \leq 120 \end{cases} \quad (9)$$

The condition for $\alpha = I_{\max}$ is $D = 1$, and the combination of $D = 1$ and α represents a high-intensity, short-duration rainfall process. As shown in Fig. 8, Eq. 9 is used to quantify the rainfall intensity threshold at which this type of rainfall process triggers a debris flow for different AEP



394 values. In Fig. 8, α (or I_{\max}) represents parabolic variation with AEP. Interestingly, α does not
 395 always decrease with continuously increasing AEP. When $AEP \leq 50$ mm, the α values necessary
 396 for triggering a debris flow increase simultaneously with AEP; when $AEP > 50$ mm, α decreases
 397 with increasing AEP, but the decrease does not continue indefinitely with increasing AEP, because
 398 for $AEP > 90$ mm, α is constant at 6.8 mm (Table 5).



399
 400 Fig. 8 Function curve describing the relationship between AEP and α

401 The key variables V_s and V_w are used to explain the quantitative evolution described by Eq. 9.
 402 To facilitate the analysis, the V_s and α values calculated by Dens-ID were normalized, and they are
 403 plotted versus AEP ($AEP-V_s$ and $AEP-\alpha$) in Fig. 9. V_s increases continuously for $AEP < 50$ mm,
 404 at which it reaches a maximum. As V_s increases with increasing AEP, a larger volume value of
 405 runoff (V_w) is required to bring the debris flow density (ρ_{mix}) to a fixed value of 2.2 or 1.2 g/cm³,
 406 which requires stronger hydrodynamic conditions, and thus a higher hourly rainfall intensity.
 407 Before point P₁ in Fig. 9, the rainfall intensity (or α) at which a debris flow occurs for $D = 1$ is
 408 positively correlated with AEP. Although AEP no longer contributes to the variation of V_s after
 409 AEP reaches 50 mm, the soil water content can still increase with continuously increasing AEP,
 410 reducing the surface infiltration rate and increasing the runoff volume generated from rainfall.



411 Under these hydrological conditions, the rainfall intensity I_{\max} (or α) required to trigger a debris
 412 flow with a fixed density value decreases gradually; thus, α is negatively correlated with AEP.
 413 When AEP exceeds 90 mm (P_2 in Fig. 9), α stops gradually decreasing and remains constant,
 414 indicating that at AEP = 90 mm, the loose solid material in JJG become saturated. Under these
 415 hydrological conditions, α has a constant value of 6.8 mm and does not change with AEP.
 416 Therefore, for the two inflection points P_1 and P_2 in Fig. 9, AEP is the external driving factor and
 417 operates through the entire process of debris flow formation in JJG, whereas the limiting
 418 conditions, maximum V_s and constant saturated soil water content (θ_s), are the two intrinsic factors.

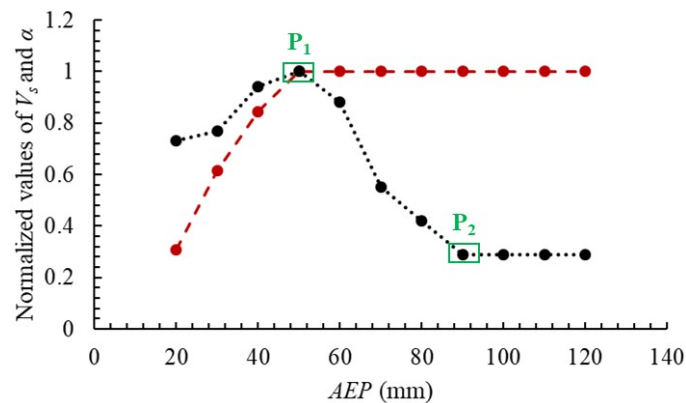


Fig. 9 AEP- α curve (black dashed line) and AEP- V_s curve (red dashed line)

421 **Effect of AEP on β :** The effect of AEP on β is described by the following equations, which
 422 were fitted using the AEP and β values in Table 5.

$$\begin{cases} \beta = -0.0079AEP - 0.35 & 20 \leq AEP < 90 \\ \beta = -0.95 & 90 \leq AEP \leq 120 \end{cases} \quad (10)$$

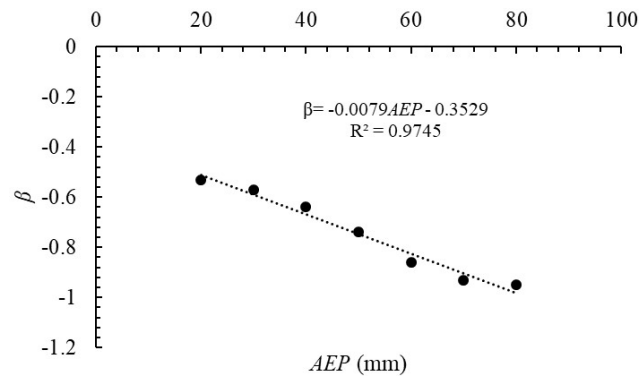


Fig. 10 Function curve describing the relationship between AEP and β for AEP values ranging from 20 to 90 mm

Eq. 10 and Fig. 10 show that as AEP increases from 20 to 90 mm, β decreases linearly. When AEP exceeds 90 mm, β becomes a constant with a value of -0.95 . These results, in combination with Eq. 9, reveal that α and β in the ID threshold equation are constant when AEP exceeds 90 mm. This result further shows that there is an interval in which AEP affects the ID threshold curve of debris flow in JJG, specifically, $AEP \in [20, 90]$.

4.4 Validation of quantitative relationship

Using the historical rainfall data in Table 3, four ID threshold curves for different AEP values were fitted, as shown Fig. 11. The green dotted line represents $AEP = 15$ mm, and the fitted equation is $I = 11.99D^{-0.45}$. The red dotted line represents $AEP = 20$ mm ($I = 10.58D^{-0.44}$). The black dotted line represents $AEP = 30$ mm ($I = 13.16D^{-0.60}$). The orange dotted line represents $AEP = 50$ mm ($I = 15.25D^{-0.78}$). These lines differ when D is larger than 3. For $D > 3$, the ID threshold curve appears lower in the $I-D$ coordinate system with increasing AEP, indicating that lower rainfall conditions will trigger debris flow. This tendency is consistent with the simulated results in Fig. 7, further demonstrating that Dens-ID may be able to describe the formation process of rainfall-induced debris flow.

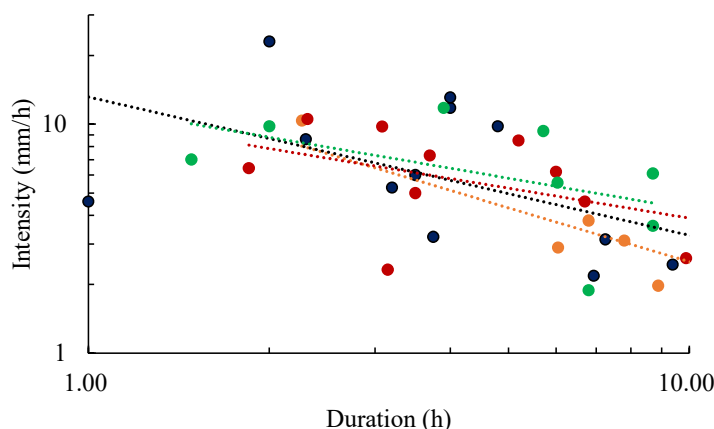


Fig. 11 Historical-data-based ID curves for different AEP values. Green, red, black, and orange symbols and lines

represent AEP values of 15, 20, 30, and 50, respectively.

The curves fitted using historical rainfall data and Dens-ID for the same AEP were drawn in separate graphs, where each graph corresponds to a different AEP value between 15 and 90 mm.

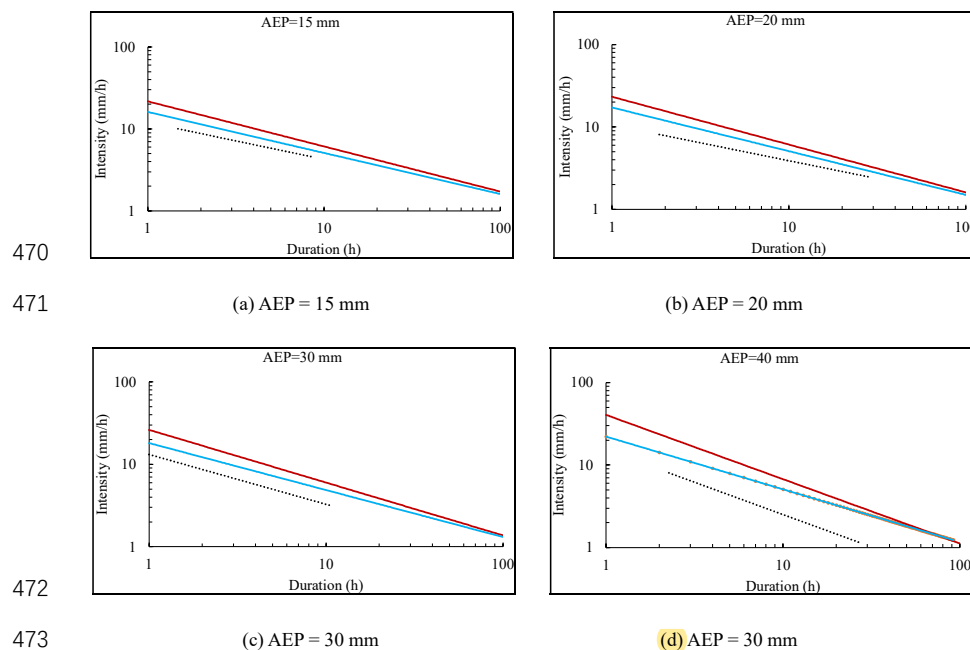
As shown in Table 2, only one debris flow event each was collected from the observation station for AEP values of 60 and 90 mm. In Fig. 12(e) and (f), the single points at which the I and D data in Table 3 coincide with the model-derived curves are indicated. These points are located between the threshold curves, which are isodensity curves corresponding to debris flow densities of 2.2 and 1.2 g/cm³. Any combination of I and D between these two isodensity curves indicates that these

rainfall conditions can trigger a debris flow. Because the closed area formed by the two curves covers historical data on rainfall that triggered a debris flow event, the curves derived by Dens-ID are at reasonable positions in I - D coordinates (that is, the α and β values that determine the position of $I = \alpha D^\beta$ in I - D coordinates are reasonable). Therefore, the α and β values of the Dens-ID-derived threshold curves corresponding to AEP values of 60 and 90 mm can be used to analyze the relationship between AEP and α and β .

Forty-three debris flow events corresponding to AEP values of 15, 20, 30, and 40 mm are



459 plotted in Fig. 12(a)–(d). Four ID threshold curves (black dashed lines) corresponding to these
 460 AEP values were fitted using the rainfall data associated with each event. In each panel, the red
 461 and blue lines are ID threshold curves fitted by Dens-ID for debris flow densities of 1.2 g/cm^3 (the
 462 upper boundary for identifying debris flow formation) and 2.2 g/cm^3 (the lower boundary),
 463 respectively (Zhang et al., 2020). If a data point representing (I, D) is above the black dashed or
 464 blue line, these rainfall conditions may trigger debris flows (Cain, 1980; Zhang et al., 2020).
 465 Although the black dashed and blue lines were fitted by different methods, both are used as lower
 466 limits for identifying debris flow formation. By using the black dashed line as a reference, the blue
 467 line can be calibrated according to its deviation from the black dashed line for each AEP value;
 468 then the errors of the equations describing the relationships between AEP and α and β (Eqs. 9 and
 469 10, respectively) can be evaluated.



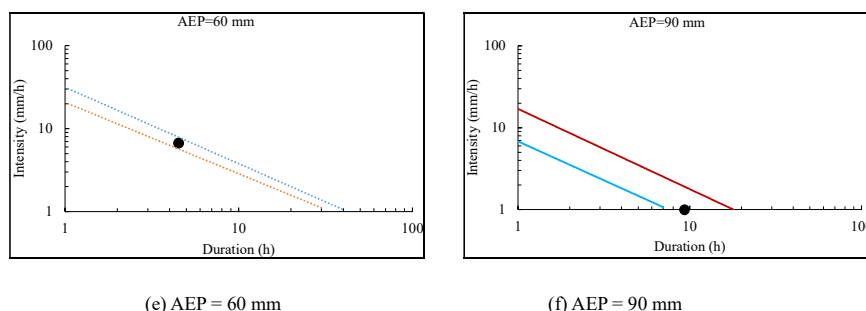


Fig. 12 ID threshold curves fitted using historical data in Table 3 (black dashed line) and Dens-ID (blue and red lines)

As shown in Table 6, the errors of α for AEP values of 40, 30, 20, and 15 mm are 39.1%, 50.1%, 27.1%, and 35.1%, respectively, and the average error is approximately 37.85%. The errors of β for AEP values of 40, 30, 20, and 15 mm are 14.6%, 21.7%, 2.30%, and 5.80%, respectively, and the average error is approximately 11.10%. According to the physical meaning of α and β , the error of Eq. 9 (approximately 37.85%) indicates that Dens-ID overestimates the triggering rainfall intensity (I_{\max}) for $D = 1$. Additionally, the calculated β values, which represent the deceleration rate of rainfall intensity with increasing rainfall duration, have a smaller error than the α values.

Table 6 Error calibration using historical data

AEP (mm)	Fitted by historical data		Fitted by Dens-ID		Error (%)	
	α	β	α	β	α	β
40	15.2	-0.78	21.15	-0.666	39.1	14.6
30	13.2	-0.6	19.81	-0.587	50.1	21.7
20	13.3	-0.52	16.91	-0.508	27.1	2.3
15	12	-0.45	14.875	-0.4685	35.1	5.8

The threshold curves fitted using historical rainfall data are below the Dens-ID fitting curves in I -



487 D coordinates for the following reasons. (1) The process of debris flow formation in the gully is
 488 extremely complex, but Dens-ID cannot fully describe this process because of necessary
 489 simplifications in the code. Consequently, the simulated data may differ from the observed rainfall
 490 data, especially the triggering rainfall intensity (I_{\max} or α) for $D = 1$. (2) According to Zhang et al.
 491 (2020, 2021), Dens-ID is sensitive to input parameters such as rainfall, hydrology parameters, and
 492 soil mechanical parameters, and it is most sensitive to soil cohesion. Unavoidable uncertainties in
 493 many input parameters for the physical model can significantly affect the calculation results of
 494 Dens-ID (Raia et al., 2014; Zhang et al., 2018; Jacobs et al., 2020). (3) Local heavy rainfall in JJG
 495 is the main trigger for debris flow. The historical rainfall data in Table 3 were obtained at the
 496 rainfall station represented by a red circle in Fig. 2, which is approximately 2 km from Menqian
 497 Gully. Because of this spatial deviation, the rain gauge may be unable to detect the center of
 498 rainstorms, and thus the measured rainfall data may be smaller than the actual values.

499 5 Conclusions

500 Rainfall simulations using Dens-ID were employed to construct a database of ID threshold
 501 curves under different AEP conditions, and this database was used to thoroughly examine the
 502 quantitative effect of AEP on the ID threshold curves. The following conclusions are drawn.

503 (1) The ID threshold curve obtained using Dens-ID can be expressed by a power function,
 504 and the R^2 values of the fitted power functions are all larger than 96%. The fitted curves from our
 505 model are all consistent in shape with the threshold curve obtained from the statistical model,
 506 indicating that the model can reflect the hydrological process of rainfall-induced debris flow with
 507 high reliability.

508 (2) The relationships between AEP and the parameters α and β can be described by



509 functions that were verified using the *ID* curves fitted using historical rainfall data for JJG. The
 510 errors of the relationships between AEP and α and β are approximately 37.85% and 11.10%,
 511 respectively. That is, Dens-ID overestimates the effects of AEP on α and β compared to those
 512 indicated by historical rainfall data. This result can be attributed to limitations on the ability of
 513 Dens-ID to describe debris flow formation, the uncertainty of the input parameters of Dens-ID,
 514 and the suitability of rain gauge data for detecting rainstorm centers.

515 (3) The two derived equations can clarify the variation of debris flow *ID* curves with AEP.
 516 The conventional *ID* threshold curve remains the same regardless of AEP once it is determined.
 517 However, the AEP can significantly affect the determination of the *ID* curve. The effects of AEP
 518 on α and β cause the originally static *ID* curve to become a variable threshold in the *I-D*
 519 coordinate system. Consequently, the *ID* curves fully reflect the effects of AEP when they are used
 520 to predict debris flow. Our study may improve the prediction precision of *ID* curves.

521 **Acknowledgement:**

522 This work was supported by the National Key Research and Development Program of China
 523 (2018YFC1505503), Project of the Department of Science and Technology of Sichuan Province
 524 (No. 2021YFG0258), National Natural Science Foundation of China (No. 42001100).

525 **References**

- 526 Adams, B., Fraser, H., Howard, C., Hanafy, M. (1986). Meteorological data analysis for drainage
 527 system design. J. Environ. Eng. 112
- 528 Baum, R.L., Savage, W.Z., and Godt, J.W. (2002). TRIGRS-a FORTRAN program for transient
 529 rainfall infiltration and grid-based regional slope stability analysis, Virginia, US Geological
 530 Survey Open file report, 02-424.



- 531 Baum, R.L., Savage, W.Z., and Godt, J.W. (2008). TRIGRS-a FORTRAN program for transient
 532 rainfall infiltration and grid-based regional slope stability analysis, Virginia, US Geological
 533 Survey Open file report, 2008-1159.
- 534 Bel, C., Liébault, F., Navratil O., Eckert N., Bellot H., Fontaine, F., Laigle, D. (2017). Rainfall
 535 control of debris-flow triggering in the Réal Torrent, Southern French Prealps, 291, 17-32.
- 536 Berti, M., Bernard, M., Gregoretti, C., Simoni, A. (2020). Physical interpretation of rainfall
 537 thresholds for runoff-generated debris flows. *Journal of Geophysical Research-Earth Surface*,
 538 125, e2019JF005513.
- 539 Berti, M., Simoni, A. (2005). Experimental evidences and numerical modelling of debris flow
 540 initiated by channel runoff. *Landslides* 3, 171–182
- 541 Caine, N. (1980). The rainfall intensity-duration control of shallow landslides and debris flows.
 542 *Geogr. Ann. Ser. A Phys. Geogr.*, 62, 23–27.
- 543 Cannon, S., Gartner, J., Wilson, R., Bowers, J., Laber, J. (2008). Storm rainfall conditions for
 544 floods and debris flows from recently burned areas in southwestern Colorado and southern
 545 California. *Geomorphology*, 96, 250-269.
- 546 Castillo, V.M., Gómez-Plaza, A., Martínez-Mena, M. (2003). The role of antecedent soil water
 547 content in the runoff response of semiarid catchments: a simulation approach. *J. Hydrol.*, 284
 548 (1–4), 114–130.
- 549 Chen, C.Y., Chen, T.C., Yu, F.C., Yu, W.H., Tseng, C.C. (2005). Rainfall duration and debris-flow
 550 initiated studies for real-time monitoring. *Environ Geol.*, 47, 715–724.
- 551 Chen, C.W., Oguchi, T., Chen, H., Lin, G.W., (2018). Estimation of the antecedent rainfall period
 552 for mass movements in Taiwan. *Environ. Ear. Sci.*, 77, 184.



- 553 Chmiel, M., Walter, F., Wenner, M., Zhang, Z., Mcardell, B.W., Hibert, C. (2020). Machine
 554 learning improves debris flow warning. *Geophysical Research Letter*, 48, e2020GL090874.
- 555 Church, M., Jakob, M. (2020). What is a debris flood? *Water Resour. Res.*, 56, e2020WR027144.
- 556 Coe, J.A., Kinner, D.A., Godt, J.W. (2008). Initiation conditions for debris flows generated by
 557 runoff at Chalk Cliffs, central Colorado. *Geomorphology*, 3, 270–297.
- 558 Crosta, G.B., Frattini, P. (2003). Distributed modeling of shallow landslides triggered by intense
 559 rainfall. *Nat. Hazards Earth Syst. Sci.*, 3, 81–93.
- 560 Cui, P., Yang, K., Chen, J. (2003). Relationship between occurrence of debris flow and antecedent
 561 precipitation: taking the Jiangjia Gully as an example, China. *J. Soil Water Conserv.*, 1, 11–15
 562 (in Chinese).
- 563 Dahal, R.K., Hasegawa, S. (2008). Representative rainfall thresholds for landslides in the Nepal
 564 Himalaya. *Geomorphology*, 100, 429–443.
- 565 Gabet, E.J., Mudd, S.M. (2006). The mobilization of debris flows from shallow landslides.
 566 *Geomorphology*, 1, 207–218.
- 567 Giannecchini, R., Galanti, Y., D'Amato, A. G. (2012). Critical rainfall thresholds for triggering
 568 shallow landslides in the Serchio River valley (Tuscany, Italy). *Nat. Hazards Earth Syst. Sci.*, 12,
 569 829–842.
- 570 Glade, T., Crozier, M.J., Smith, P. (2000). Applying probability determination to refine landslide-
 571 triggering rainfall thresholds using an empirical “Antecedent Daily Rainfall Model”. *Pure Appl.*
 572 *Geophys.*, 157, 1059–1079.
- 573 Guo, X.J., Cui, P., Li, Y. (2013). Debris flow warning threshold based on antecedent rainfall: a
 574 case study in Jiangjia Ravine, Yunnan, China. *J. Mount. Sci.*, 10, 305–314.



- 575 Guzzetti, F., Peruccacci, S., Rossi, M., Strak, C.P. (2008). The rainfall intensity–duration control
 576 of shallow landslides and debris flows: an update. *Landslides*, 5, 3-17.
- 577 Hasnawir, Kubota, T. (2008). Analysis of critical value of rainfall to induce landslides and debris-
 578 flow in Mt. Bawakaraeng Caldera, South Sulawesi, Indonesia. *J. Fac. Agric. Kyushu Univ.*, 53,
 579 523-527.
- 580 Hirschberg, J., Badoux, A., McArdell, B.W., Leonarduzzi, E., Molnar, P. (2021). Evaluating
 581 methods for debris-flow prediction based on rainfall in an Alpine catchment. *Nat. Hazards Earth*
 582 *Syst. Sci.* 21, 2773-2789.
- 583 Iverson, R. M., Reid, M. E., LaHusen, R. G. (1997). Debris flow mobilization from landslides.
 584 *Annu. Rev. Earth Planet.*, 25, 85-138.
- 585 Jacobs L., Kervyn, M., Reichenbach, P., Rossi, M., Marchesini, I., Alvioli, M., Dewitte, O., 2020.
 586 Regional susceptibility assessments with heterogeneous landslide information: Slope unit- Vs.
 587 pixel-based approach. *Geomorphology*, 356: 107084.
- 588 Jiang, Z.Y., Fan, X.M., Subramanian, S.S., Yang, F., Tang, R., Xu, Q., Huang, R.Q. (2021).
 589 Probabilistic rainfall thresholds for debris flows occurred after the Wenchuan earthquake using
 590 a Bayesian technique. *Eng. Geo.*, 280, 105965.
- 591 Jones, R., Thomas, R.E., Peakall, J., Manville, V. (2017). Rainfall-runoff properties of tephra:
 592 Simulated effects of grain-size and antecedent rainfall. *Geomorphology*, 282, 39-51.
- 593 Khan, Y.A., Latch, H., Baten, M.A., Kamil, A.A. (2012). Critical antecedent rainfall conditions for
 594 shallow landslides in Chittagong City of Bangladesh. *Environ. Earth Sci.*, 67, 97-106.
- 595 Kim, S.W., Chun, K.W., Kim, M., Catani, F., Choi, B., Seo, J. (2021). Effect of antecedent rainfall
 596 conditions and their variations on shallow landslide-triggering rainfall thresholds in South



- 597 Korea. Landslides, 18, 569-582.
- 598 Kim, S.K., Hong, W.P., Kim, Y.M. (1991). Prediction of rainfall-triggered landslides in Korea. In:
- 599 Bell DH (ed) Landslides, Proceedings of the 6th International Symposium on Landslides, vol 2.
- 600 Balkema, Rotterdam, pp 989-994.
- 601 Le Bissonnais, Y., Renaux, B., Delouche, H. (1995). Interactions between soil properties and
- 602 moisture content in crust formation, runoff and interrill erosion from tilled loess soils. Catena,
- 603 25(1), 33-46.
- 604 Lehmann, P., Or, D. (2012) Hydromechanical triggering of landslides: From progressive local
- 605 failures to mass release. Water Resour. Res., 48, W03535.
- 606 Liu, D.L., Zhang, S.J., Yang, H.J., Zhao, L.Q., Jiang, Y.H., Tang, D., Leng, X.P. (2016).
- 607 Application and analysis of debris-flow early warning system in Wenchuan earthquake-affected
- 608 area. Nat. Hazards Earth Syst. Sci., 16, 483-496.
- 609 Long, K., Zhang, S.J., Wei, F.Q., Hu, K.H., Zhang, Q., Luo, Y. (2020). A hydrology-process based
- 610 method for correlating debris flow density to rainfall parameters and its application on debris
- 611 flow prediction. Journal of Hydrology, 589, 125124.
- 612 Luk, S.H. (1985). Effect of antecedent soil moisture content on rainwash erosion. Catena, 12, (2–
- 613 3), 129–139.
- 614 Marno, P., Peres, D.J., Cancelliere, A., Greco, R., Bogaard, T.A. (2020). Soil moisture information
- 615 can improve shallow landslide forecasting using the hydrometeorological threshold approach.
- 616 Landslides, 17, 2041-2054.
- 617 Marra, F., Destro, E., Nikolopoulos, E.I., Zocatelli, D., Creutin, J.D., Guzzetti, F., Borga, M.
- 618 (2017). Impact of rainfall spatial aggregation on the identification of debris flow occurrence



- 619 thresholds. Hydrol. Earth Syst. Sci., 21, 4525-4532.
- 620 Minder, J.R., Roe, G.H., Montgomery, D.R. (2009). Spatial patterns of rainfall and shallow
 621 landslide susceptibility. Water Resour. Res., 45, W04419.
- 622 Oorthuis, R., Hurlimann, M., Abanco, C., Moya, J., Carleo, L. (2021). Monitoring of rainfall and
 623 soil moisture at the Rebaixader catchment (Central Pyrenees). Environmental & Engineering
 624 Geoscience, 27(2), 221-229.
- 625 Papa, M.N., Medina, V., Ciervo, F., Bateman, A. (2013). Derivation of critical rainfall thresholds
 626 for shallow landslides as a tool for debris flow early warning systems. Hydrol. Earth Syst. Sci.
 627 17, 4095-4107.
- 628 Peres, D.J., Cancelliere, A. (2014). Derivation and evaluation of landslide-triggering thresholds by
 629 a Monte Carlo approach. Hydrol. Earth Syst. Sci., 18, 4913-4931.
- 630 Raia, S., Alvioli, M., Rossi, M., Baum, R.L., Godt, J.W., Guzzetti, F., 2014. Improving predictive
 631 power of physically based rainfall-induced shallow landslide models: a probabilistic approach,
 632 Geosci. Model Dev., 7, 495-514.
- 633 Richards, L.A., 1931. Capillary condition of liquids in porous mediums. Physics 1, 318-333.
- 634 Ruetze, J.V., Lehmann, P., Or, D. (2014) Effects of rainfall spatial variability and intermittency on
 635 shallow landslide triggering patterns at a catchment scale. Water Resour. Res., 50, 7780-7799.
- 636 Segoni, S., Piciullo, L., Gariano, S.L. (2018). A review of the recent literature on rainfall
 637 thresholds for landslide occurrence. Landslides, 15, 1483-1501.
- 638 Theule, J.I., Liébault, F., Laigle, D., Loye, A., Jaboyedoff, M. (2015). Channel scour and fill by
 639 debris flows and bedload transport. Geomorphology, 243, 92-105.
- 640 Tisdall, A. (1951). Antecedent soil moisture and its relation to infiltration. Aust. J. Agric. Res., 2



- 641 (3), 342–348.
- 642 Yang, H.J., Wei, F.Q., Ma, Z.F., Gao, H.Y., Su, P.C., Zhang, S.J. (2020). Rainfall threshold for
 643 landslide activity in Dazhou, southwest China. *Landslides*, 17, 61-77.
- 644 Zhang, S.J., Jiang, Y.H., Yang, H.J., Liu, D.L. (2015). An hydrology-process based method for
 645 antecedent effect rainfall determination in debris flow forecasting. *Adv. Water Sci.*, 26, 35-43.
 646 (In Chinese)
- 647 Zhang, S.J., Ma, Z.G., Li, Y.J., Hu, K.H., Zhang, Q., Li, L. (2021). A grid-based physical model to
 648 analyze the stability of slope unit. *Geomorphology*, 391, 107887.
- 649 Zhang, S.J., Wei, F.Q., Liu, D.L., Yang, H.J., Jiang, Y.H. (2014b). A regional-scale method of
 650 forecasting debris flow events based on water-soil coupling mechanism. *J. Mount. Sci.*, 6, 1531-
 651 1542.
- 652 Zhang, S.J., Xu, C.X., Wei, F.Q., Hu, K.H., Xu, H., Zhao, L.Q., Zhang, G.P. (2020). A physics-
 653 based model to derive rainfall intensity-duration threshold for debris flow. *Geomorphology*, 351,
 654 106930.
- 655 Zhang, S.J., Yang, H.J., Wei, F.Q., Jiang, Y.H., Liu, D.L. (2014a). A model of debris flow forecast
 656 based on the water-soil coupling mechanism. *J. Earth Sci.*, 4, 757-763.
- 657 Zhang, S.J., Zhao, L.Q., Delgado Tellez, R., Bao, H.J. (2018). A physics-based probabilistic
 658 forecasting model for rainfall-induced shallow landslides at regional scale. *Nat. Hazards Earth*
 659 *Syst. Sci.*, 18, 969-982.
- 660 Zhao, B.R., Dai, Q., Han, D.W., Dai, H.C., Mao, J.Q., Mao, J.Q., Zhuo, L. (2019). Probabilistic
 661 thresholds for landslides warning by integrating soil moisture conditions with rainfall thresholds.
 662 *Journal of Hydrology*, 574, 276-287.